Available online at https://rsgmodelling.co.uk/
Commun. Nonlinear Anal. 12 (2) (2024), 27–41
Research Article

**Communications in Nonlinear Analysis**
Publisher
Research & Scinece Group Ltd.

# Heat Transfer During Cellular Magnetoconvection in Liquid Gallium

Md Abdul Rawoof Sayeed

*Department of Mathematics, Muffakham Jah College of Engineering and Technology, Bangara Hills, Road No #3, Hyderabad, India*

Hakeemuddin Ahmed

*Department of Mechanical Engineering, Moulana Azad National Urdu University, Polytechnic, Kadapa, A.P, India*

**Abstract**

The effect of a vertically applied magnetic field on the heat transfer in a liquid Gallium layer at the onset of stationary convection is studied analytically by using the stress-free boundary conditions in this paper. Investigations are carried out to determine the heat transfer rate up to eight by adopting the approach of Kuo [9] that utilizes the expansion of thermal Rayleigh number ($R$). The results of the flow field are shown in the form of streamlines and the heat transfer characteristic is depicted as isotherms. The heat function concept was utilized to follow the path of convective heat transport in the liquid Gallium layer, which serves well to interpret the distribution of energy comprehensively in terms of heatlines. It is also shown that total energy (kinetic and potential energy) is reduced in liquid gallium due to the application of a vertical magnetic field. It is also shown that total energy (kinetic and potential energy) is reduced in liquid gallium due to the application of a vertical magnetic field.

*Keywords:* Liquid Gallium, thermal convection, electrically conducing fluid, magnetic field, Nusselt number, heat function
*2010 MSC:* 35K05, 76Rxx

## 1. Introduction

Generally, liquid metals are distinguished by their large values of magnetic diffusivity when compared to their thermal diffusivity. Consequently, these metals lend themselves to studies related to fluids with low Prandtl numbers (magnetic Prandtl numbers $Pr_2$ have values of order $10^{-7}$). Due to small values of $Pr_2$, the magnetic Reynolds number ($Pr_2/Pr_1$) is vanishingly small and the predominant effect of the applied magnetic field is faster dissipation of mechanical energy as a result of Ohmic heating.

*Email addresses:* rfsayeed@mjcollege.ac.in (Md Abdul Rawoof Sayeed), hakeemuddin@manuu.edu.in (Hakeemuddin Ahmed)

*Received 2024-04-24*

During the initial stages of convective flow in liquid metals, the two-dimensional steady roll structures transform quickly into time-dependent structures just above the critical stationary Rayleigh number, $R = R_{sc}$. In a horizontal layer of liquid metal, the thermal convection flow is suppressed depending upon the magnitude of an external magnetic field. There is a critical magnitude for this magnetic field, above which convective flow is inhibited. When the magnitude of the applied magnetic field strength passes through this critical value, the magnetic field force and buoyancy counteract each other. oscillations occur in the liquid metal for these reasons. The majority of experimental studies on liquid metal convection have concentrated on measuring the system's heat transport and temperature fluctuations at various points in the liquid layer caused by turbulence [6]-[14]. Thus experiments using liquid metals are of great value in assessing the effects of high electrical and thermal conductivity.

In this magnetoconvection study, liquid gallium is considered as the working fluid. Gallium has excellent characteristics such as low toxicity, low vapour pressure and low melting point when compared to mercury or liquid Sodium which make it safer and easier to work with. On the other hand, liquid gallium does pose some problems during experimentation as it dissolves many metals and oxidises readily in air.

In liquid gallium, both the Prandtl numbers are significantly less than unity and further, the magnetic Prandtl number ($Pr_2 = 1.5 \times 10^{-6}$) is much less than the thermal Prandtl number ($Pr_1 = 0.021 - 0.023$). similar to the earth's core and stationary convection is expected at the onset of convection.

The process of magnetoconvection plays a vital role during the crystal growth from the melt. Generally, the buoyancy force induced by the thermal and solutal gradients acts as a driving force for the convection currents in the melt. The application of magnetic field leads to the damping of both flow and temperature oscillations in the melt and thereby provides a promising opportunity to enhance the quality of the crystals formed [12].

Jalal et.al. [4] have numerically studied the three-dimensional turbulent natural convection with heat transfer $R = 10^8$ in molten sodium under the influence of a uniform magnetic field. They have used the $k - \epsilon$ turbulence model for $R = 10^8$. The effect of a magnetic field on the average Nusselt number for $R = 10^6$ in two-dimensional flow was compared with that of the three-dimensional flow. Juel et.al. [5] presented their experimental and numerical study of the effects of a steady magnetic field on sidewall convection in molten gallium. They showed that when the magnetic field was applied across the main flow, it reduced the convection effects and they also proved that their results were in good agreement when this effect was scaled with the relevant parameters.

The measurement of the heat flux passing through the gallium is of the utmost importance and requires consideration during experimentation. Arnou and Olson [1] investigated the thermal convection process in a low Prandtl number($Pr = 0.023$), electrically conducting fluid. A liquid Gallium layer was subjected to uniform rotation and a uniform vertical magnetic field was applied to measure the heat transfer rate. For Rayleigh-Benard (non-rotating, non-magnetic) convection a Nusselt number($N$)-Rayleigh number law $N = 0.129 \times R^{0.272\pm0.006}$ was obtained. In the case of non-rotating magnetoconvection, it was found that the critical Rayleigh number $R_c$ increased linearly with magnetic energy density, and the heat transfer was governed by the expression $N \approx R^{1/2}$. In the present study, the authors have adopted Kuo's [9] approach to analyse the characteristics of magnetoconvection with stress-free boundary conditions in the layer of liquid gallium at the start of the stationary convection process. This is an extensive study of the magnetoconvection process involving the physical parameters about liquid gallium by adopting the methodology of numerical studies carried out by Rameshwar et.al. [13].

Section 2 deals with the equations that are associated with the Boussinesq magnetoconvection in RBC(Rayleigh-Benard convection). The finite-amplitude fields of temperature and velocity are determined by the recurring method of solution, which is described in Section 3. These nonlinear equations were then solved by expanding the variables introduced by Kuo [9] in Section 4. The Section 5 examines the numerical results in relation to $N$, which is affected by $R$, $Q$Chandrasekar Number, $Pr_1$ and $Pr_2$. Section 6 shows the distorted patterns of streamlines and isotherms for various values of physical parameters pertaining to liquid gallium. The heat function and the corresponding heatline patterns are discussed in Section 7. The conclusions are finally presented in Section 8.

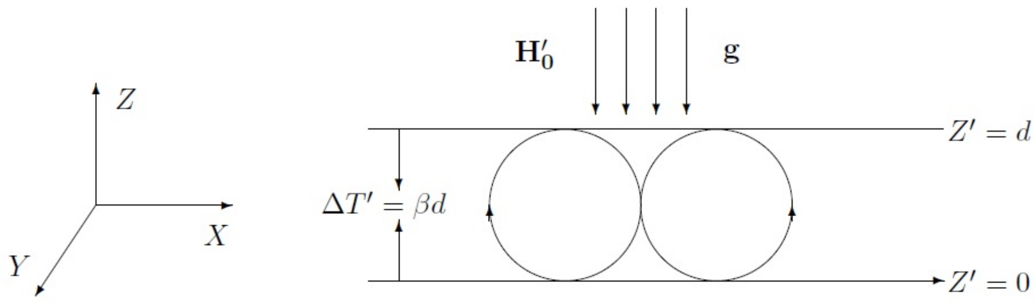


Figure 1: Schematic diagram of the physical model

## 2. Mathematical Model

In the present study, let us consider two infinite horizontal planes with adverse temperature gradient $\Delta T'$ as shown in Fig.1. An electrically conducting fluid is considered between these planes and it is assumed that a magnetic field, $\mathbf{H}_o^{'} = H_o^{'}\hat{\mathbf{e}}_\mathbf{z}$ is applied externally perpendicular to the direction of these planes. The perturbed primary governing equations in non-dimensional form with Boussinesq approximation, are given by,

$$\nabla.\mathbf{V} = 0, \nabla.\mathbf{H} = 0, \tag{2.1}$$

$$\frac{1}{Pr_1}\left[\frac{\partial \mathbf{V}}{\partial t} + (\mathbf{V}.\nabla)\,\mathbf{V}\right] - Q\frac{Pr_2}{Pr_1}(\mathbf{H}.\nabla)\mathbf{H} = -\nabla\left(\frac{P_1}{Pr_1} + \frac{QPr_2}{2Pr_1}|\mathbf{H}|^2 + QH_z\right) + Q\frac{\partial \mathbf{H}}{\partial Z} + Ra\theta\hat{\mathbf{e}}_\mathbf{z} + \nabla^2\mathbf{V}, \tag{2.2}$$

$$\left(\frac{\partial}{\partial t} - \nabla^2\right)\theta = w - (\mathbf{V}.\nabla)\,\theta, \tag{2.3}$$

$$\left(\frac{Pr_2}{Pr_1}\frac{\partial}{\partial t} - \nabla^2\right)\mathbf{H} = \nabla\times(\mathbf{V}\times\hat{\mathbf{e}}_\mathbf{z}) + \frac{Pr_2}{Pr_1}\nabla\times(\mathbf{V}\times\mathbf{H}), \tag{2.4}$$

where $Ra = \alpha g\beta d^4/\kappa\nu$, $Q = \mu_m H_o^2 d^2/4\pi\rho_o\nu\eta$, $Pr_1 = \nu/\kappa$ and $Pr_2 = \nu/\eta$. In Eqs. (2.1)-(2.4), $\theta(= T - T_s)$, $\mathbf{V}$ and $\mathbf{H}$ denote the perturbed unknowns for temperature, velocity and magnetic field, respectively. In this study, the boundary conditions are considered to be stress-free as assumed in [[2], which can be written as,

$$w = \frac{\partial^2 w}{\partial Z^2} = \theta = 0, H_X = H_Y = 0 \quad \text{and} \quad \frac{\partial H_Z}{\partial Z} = 0 \quad \text{at} \quad Z = 0, 1. \tag{2.5}$$

The equations (2.1-2.4) along with the boundary condition (2.5) were solved by an approach similar to the one adopted by Rameshwar et.al. [13].

## 3. Convective heat transport and Average Nusselt number $N$

The average heat transport along the horizontal direction is calculated by using $N$ which is given by,

$$N = \overline{wT} - \frac{\partial \bar{T}}{\partial Z}, \tag{3.1}$$

where the bar in Eq. (3.1) signifies a horizontal mean. The $2^nd$, $4^th$ and $6^th$ order approximations of $N$ are denoted as $N^{(2)}$, $N^{(4)}$ and $N^{(6)}$, respectively were evaluated by an approach similar to the one adopted by Rameshwar et.al. [13].

The variation of $N$ in the absence of a magnetic field is depicted in Fig. 2(a) concerning $R$ for liquid gallium corresponding to the values of $Pr_1 = 0.021$ and 0.025. The $Pr_1$ values are the same as those considered by Aurnou and Olson [1]. According to Aurnou et.al., the values of $Pr_1$ for liquid gallium range from 0.021 to 0.025. The heat flow is observed to decrease as $Pr_1$ increases. It is quite clear that applying a magnetic field to the RBC reduces energy in motion and heat transport. For $Pr_1 = 0.021, 0.25$, the corresponding power law equations are $Pr_1 = 0.021,\quad 0.25$ are $N = 0.972(R/R_o)^{1.831}$ and $N = 0.850(R/R_o)^{1.730}$. It is worth noting that as $Pr_1$ values increase, so does the exponent of power law and the slope of the curve.

The Fig. 2(b) depicts the relationship between $N$ and $R$ for various values of $Q$, $Pr_1$ and $Pr_2$. The figure shows that by increasing $Q$ the onset of convection changes to larger $R$ values. Amplifying $Q$ for a constant $R$ causes an attenuation in convective heat transport. As a result, a vertically applied magnetic field causes a dampening effect on heat transport during convection. The power law equation for $Q = 5000$ is $N = 1.182(R/R_o)^{0.681}$, for $10^4$ is $N = 1.188(R/R_o)^{0.780}$ and for $10^5$ is $N = 1.258(R/R_o)^{0.841}$. It is evident that as $Q$ enhances, the exponent of the power-law also increases, and so does the onset of convection.

Fig. 2(c) depicts the effect of $Pr_1$ on $N$ in the presence of a magnetic field for $Q = 5000$. The heat transfer during convection across the layer in fluid is represented in this figure by a graph of $R$ versus $N$ for $Pr_1$ values pertaining to liquid gallium. It can be observed that higher values of $Pr_1$ result in more heat transfer.

Fig. 3(a) shows the variation of kinetic and potential energy with respect to $R/R_0$ for different values of $Q$ and for given values of $Pr_1 = 0.025$ and $Pr_2 = 0.15 \times 10^{-6}$ [10]. Aurnou and Olson [1] have discussed the effect of the application of vertical magnetic field for values of $Q$ ranging from 0 to 1210 on liquid gallium. For a given value of $R$, any increase in $Q$ always results in a decrease in kinetic as well as potential energy. Thus, it can be stated that the presence of a vertical magnetic field has a damping effect on the total energy of the system.

Fig. 3(b) is plotted between kinetic and potential energy and $R/R_0$ for various values of $Pr_2$ while $Pr_1$ and $Q$ values are kept constant. It can be observed from this figure that as $Pr_2$ increases the kinetic or potential energy shifts to higher values of $R$. For a given value of $R$, amplifying $Pr_2$ always leads to an attenuation during convective heat transport. Hence, it can be stated that an increase of $Pr_2$ has a damping effect on the total energy of the system.

## 4. Patterns of streamlines and distortion of isotherms

This section describes the nonlinear behaviour of the chosen system qualitatively using streamlines and isotherms. Streamlines are defined as curves that are tangential to the flow's instantaneous velocity vector. These show the fluid element's direction at any time. The shape of streamlines is either a curved path or a straight line, depending on the type of fluid flow. These provide a detailed view of the flow field's characteristics. In contrast, at any given time, the location of all points with the same temperature is represented by a curve known as an isotherm. Once interpreted, these findings can be applied to more complex structures and patterns. The stream function ($\psi$) is selected to satisfy the continuity equation.

$\nabla.\mathbf{V} = 0$. Integrating the following equations yields the value of $\psi$, which is used to plot the streamlines [13].

In the present study, we examined the flow field and temperature field for liquid gallium by showing the steady-state version of the streamline and isotherm. For given values of $Pr_1 = 0.025$ and $Pr_2 = 0.15 \times 10^{-6}$, Fig. 4-6 depict the gross characteristics of the streamlines and isotherms due to the variation of $Q$ and $R$ respectively. Figure 4(a) shows a snapshot of streamlines for $Q = 0$. This figure shows that at the onset of convection, the fluid flow is characterized by cellular patterns when $Q = 0$. Since the primary heat transfer method is convection, the forces of buoyancy are large enough to overcome the forces of viscous and thermal inertia in the fluid. As illustrated in Fig.4(a), both the absolute minimum $(0.99869 \times 10^{-7})$

and the maximum (0.0489) of the cell's circulation strength are between $0 < X < 1.4$. The isotherms at the onset of Fig.4(b) illustrate the corresponding temperature field effect. When the temperature is higher on the lower plate than the temperature on the upper plate (see Fig. 4(b)), the liquid gallium layer on the left moves to the hot plate, and the fluid layer on the right moves to the lower temperature upper plate. When the temperature is lower on the cold wall, the relatively cold liquid gallium layer moves along the right side of the cold wall, and then down towards the higher temperature wall. The isotherms on the aligned plates are almost parallel, suggesting that conduction dominates the heat transfer mode. However, there is a conduction-dominant mode change close to the bottom surface where isotherms start.

Figure 4 (c) and (d) shows the streamlines and the isotherms for liquid gallium ($Q = 670$). The flow regime changes due to a magnetic field. The magnetic effect and the buoyancy force contribute to the gravitational buoyancy of the liquid gallium. Due to the magnetic susceptibility of the fluid layer, the magnetic field attracted the relatively cooler fluid layer. The bicellular pattern changes into a multicellular pattern. The multicellular pattern separates the stream at the core as shown in Figure 4(c). As shown in Fig. 4(c), the absolute values of circulation strength for a cell are found to vary between the maximum (0.103) and minimum ($0.49993 \times 10^{-7}$ )lie in the range of $0 < X < 0.6$. The Isotherms can be used to infer the corresponding phenomenon, as shown in Fig. 4(d). The pattern of isotherms in Fig. 4(d) clearly indicates that within the fluid layer, the mode of heat transfer is convection.

As the applied magnetic field strength increases, it leads to the reorganization of the flow field which is illustrated by the contours of the instantaneous streamlines and the isotherms which is depicted in Figs. 4(e) and 4(f). The applied magnetic field has a strong effect on the streamlines, as shown in Fig. 4(e). These are the curves for $Q = 1210$. As shown in Fig. 4(e), the absolute minimum and absolute maximum values are $(0.5120 \times 10^{-7})$ and (0.101) of circulation strength for a cell lie in the range of $0 < X < 0.5$.

When Q increases from 680 to 1210, the closed cell streamline pattern increases from 6 to 7 in Fig. 4(c) and Fig. 4(e) in the region under study. However, the magnetic field induces isotherms to show sinusoidal patterns at the start of stationary convection. As a consequence, the effect of increasing the magnetic field on isotherm patterns is moderate at first.

Initially, the streamlines and isotherms of liquid gallium exhibit mild nonlinear behaviour ($R \simeq R_o$). In addition, strong flow concentrations appear at the sides, causing strong anti-eddy regions that grow until they quench the central vortex. When the isotherms form straight lines near the horizontal planes, a gap occurs. Furthermore, the Nusselt number approaches unity after which the distorted field dominates to cause a flow reversal.

As shown in Figs. 4(a, c, e), the strength of the recirculation pattern decreases, consequently, the strength of the vortex decreases as $Q$ increases. As $Q$ increases from 0 to 1210, the Lorentz force becomes stronger than the viscous force, which stabilizes the convection process of heat transfer in liquid gallium. The flow in the axial plane consists of a series of counter-rotating vortices. For a given $Q$, the absolute value of the rotational force of each cell is found to be uniform. As $Q$ increases, the width of these rolls decreases and consequently, a decrease in their wavelength is observed. This phenomenon of compressing the field lines at maximum velocity occurs when the Lorentz force acts back to compress the flow, creating counter-eddies and ultimately reversing the velocity.

Figure 5 depicts the variation in flow pattern as a result of higher values of $R$, such as $3R_o$, as the magnetic field strength increases from $Q = 0$ to $Q = 1210$, using streamlines and isotherms with $Pr_1 = 0.025$ and $Pr_2 = 0.15 \times 10^{-6}$. When $R \simeq R_o$, the current flow system mainly consists of several symmetrical parallel rolls in the horizontal layer near the supercritical buoyancy force, as shown in Figures 4(a, c, e). However, when R is increased to $3R_o$, these patterns transform into symmetric deformed roll patterns, as shown in Figs. 5(a,c,e). It is also observed that as the value of $R$ is increased further, the family of trajectories continuously transforms into another family while maintaining its motion orientation in the phase plane.

The present study assumes that circulation strength is positive in the anti-clockwise direction. As shown in Fig. 4(a), $R \simeq R_o$ has a couple of cells with positive and negative strengths of 0.0489. The preceding analysis examines the disintegration of a vortex between $0 < X < 1.4$ into multiple vortices and their subsequent merging during the flow. Figure 5(a) shows the presence of vortices in liquid gallium with

$R = 3R_o$ in the absence of a magnetic field. The circulation strength of a cell ranges from $0 < X < 1.4$, with maximum (80.53) and minimum (-80.53) values. This diagram shows 9 vortices, numbered I-IX, as well as $A, A', B$, and $B'$, all located in $0 < X < 1.4$. Similar vortices, I and II, with the same strength of 80.53, are generated by the top and bottom walls at $B$ and $B'$, respectively, close to the ones that exist. As $R$ increases, convection takes over, and fluid particles near the hot and bottom boundaries rise, causing vortex II. The denser particles near the top boundary proceed downward as a result of gravitational force, forming Vortex I. These vortices try to stretch and contract the cells (III) in the center of the cell, causing them to become strongly distorted at the lower and upper boundaries. With clockwise circulation, the distorted curved cell, III, envelopes the diagonally opposite neighbouring family of 4 vortices, $A$ and $A'$. These vortices have a negative circulation strength of 80.53. Apart from the vortices I-III mentioned above, there are four small supplementary vortices, IV and V of negative circulation strength 15.13, and VI and VII of negative circulation strength 20.13, in an anticlockwise direction to the right and left of the region's center, respectively. Further, it can also be observed that there are two smaller vortices, VIII and IX, close to the upper and lower boundaries, with a positive circulation strength of 8.20.

The Fig. 4(c) depicts the existence of a series of vortices for $R = 3R_o$ under the influence of a vertical magnetic field, $Q = 670$ with $Pr_1 = 0.025$ and $Pr_2 = 0.15 \times 10^{-6}$. The minimum (-3.60) and maximum (3.60) values of the circulation strength of a cell are found to lie between $0 < X < 0.6$. It can be observed that the three vortices, I-III, as well as the vortices $A$ and, $A'$ are located between $0 < X < 0.6$. Figure 4(c) depicts the presence of 3 vortices, I-III, as well as the vortices $A$ and $A'$ located between $0 < X < 0.6$. Apart from the existing vortices, the other vortices, I and II, of equal circulation strength of 3.00 are induced from the upper and lower walls respectively. As $R$ increases, convection takes over and the fluid particles near the relatively hotter lower boundaries rise, inducing the vortex II. As explained earlier, the downward movement of the denser particles from the upper boundary leads to the formation of vortex I. Vortices transform and contract cells (III) in the center, causing significant distortion at their boundaries. Because of the clockwise circulation, the distorted cell III envelopes the diagonally opposite neighbouring two vortices, $A$ and $A'$. The negative circulation strength of these vortices is 3.60. It can be observed from Fig. 4(c) that under the influence of the magnetic field, the cell is distorted relatively less and has three vortices. This is in contrast to the nine cells that were obtained in the absence of the magnetic field for the given set of parameter values as shown earlier in Fig. 4(a). It demonstrates that a magnetic field dampens convection in liquid gallium and stabilises the system.

The Fig. 4(e) depicts the streamlines for the set of parameters i.e., $Q = 1210$, $R = 3R_o$, $Pr_1 = 0.025$ and $Pr_2 = 0.15 \times 10^{-6}$. It can be observed from this figure that there are three major vortices, I-III, that lie between $0 < X < 0.5$. The three vortices in this case with a maximum and minimum circulation strength of 4.07 and -4.07 are similar to that obtained when $R = 3R_o$ and $Q = 670$. In the central region, vortex III envelops two vortices $A$ and $A'$ having the same strength of -4.07. As shown in Fig.4(c), this central vortex, III gradually strengthens from 3.60 to 4.07 in comparison to the central region, vortex III. The vortices I and II, with positive strengths of 0.78 near the upper and lower boundaries, also extend towards the layer's core. As shown in Figs. 4(c) and 4(e), the intensity of the induced vortices I and II decreases from 3.00 to 0.78 as the applied magnetic field increases from $Q = 670$ to $Q = 1210$. The preceding observation implies that vortex expansion with increasing buoyancy is primarily caused by vortices disintegrating and then merging during the flow. As the value of $R$ is increased further, the same pattern is observed with minor variations and increased circulation strength in the recirculation regions.

In amplifying $R$, the velocity and thermal fields show similarities concerning the heating rate. Convection is the dominant mode of heat transfer within the region, with the bottom wall transferring the vast majority of heat. Figure 4(b) depicts the inputs derived from the core thermal plumes, as well as the produced updrafts and downdrafts, which are distinguished by small local vortices. In this case, buoyancy forces become comparable to viscous forces, signalling the onset of heat transfer in the convective mode. However, $R$ is increases more than $3R_o$ then the heat transfer mode shifts from conduction to convection. In this case, the isotherms are not smooth curves but are rather dispersed throughout the layer, resulting in slithering structures as shown in (Figs. 4(b, d, f)). From the preceding observations, it is quite evident that the heating rate has a significant effect on the flow pattern of the vortex, which impacts the circulation strength of the fluid flow.

Figure 5 shows the isotherms and streamlines for different values of Q, $R = 5R_o$, $Pr_1 = 0.025$, and $Pr_2 = 0.15 \times 10^{-6}$. The Figs. 5(a, b) show the streamlines and isotherms plots for a given set of parameters in the absence of a magnetic field, $Q = 0$. The vortex pattern in Fig. 4(a) plotted for $R = 3R_o$ becomes more deformed for $R = 5Ro$, indicating that viscosity dissipation increases with an increase in $R$, and thus chaotic behaviour of the fluid increases, as shown in Fig. 5. (a). In Fig. 5(a), a total of 11 counterclockwise circulating vortices can be observed which has additional two vortices when compared with Fig. 4(a).

The circulation of the upper and lower wall-induced vortices I and II increases from 80.53 at $B$ and $B^{'}$ to 411.89. The negative circulation strength central vortex, III also enhanced from min -80.53 to min -411.89. The circulation strengths of the other two pairs of small vortices in the middle region (IV, V) and (VI, VII), are also enhanced from 15.13 to 70.71 and 20.13 to 102.80. Additionally, two new vortices are induced near upper and lower boundaries beside the existing vortices VIII and IX, namely X and XI with a minimum circulation strength of -95. Further, the buoyancy forces begin to dominate the viscous forces, increasing the strength of the vortex and generating new vortices. It is interesting to note that the streamlines are scattered in the entire flow region for $R = 5R_o$, as buoyancy forces dominate over the viscous forces. A similar phenomenon for streamlines can be inferred from Figs. 5(c, e) in comparison to Figs. 4(c, e) under the influence of magnetic field in liquid gallium. It is observed that in the central region, the isotherms are compressed close to the boundaries for high values of $R$. The wavy pattern in Figs. 5(b, d, f) is caused by different levels of compression of isotherms, which results in the formation of multiple circulation cells. These oscillations are due to the multiple circulation cells in the cavity, as shown in Fig. 5(b, d, f). Isotherms exhibit oscillations and compressions near the boundaries as well as in the central region's intermediary positions. It is fascinating to see how the streamlines and isotherms inside the region mirror each other, and how the isotherms are even, monotonic curves symmetric with respect to the middle axis.

## 5. Heat function

The numerical visualisation of heatlines is beneficial to analyse the characteristics of heat flow and to get an insight into the physics of convective heat transfer process. The heatfunction (($H^*$) for the present non-dimensional convection problem under study can be expressed as:

$$\frac{\partial H^*}{\partial x} = wT - \frac{\partial T}{\partial z}, \tag{5.1}$$

$$-\frac{\partial H^*}{\partial z} = uT - \frac{\partial T}{\partial x}, \tag{5.2}$$

where $T = T_s + \theta$ and $T_s = T_o - z$ is referred to as static temperature. Here $T_o$ is the arbitrary reference temperature that has a direct influence on the heatlines. The methodology of Rameshwaret. al. [13] is applied to solve the above equation. The heat transfer in a convective system is analysed by means of graphical representation of heatlines.

### *5.1. Results and discussion for Heatlines*

The presence of a closed loop heatline can be observed from the heatlines pattern (refer Fig. 6(b)) in the central zone for $T_o = 3$. This means that larger $T_o$ values ($T_o = 3$) lead to higher convective heat transfer in the center than smaller $T_o$ values ($T_o = 1$). The sign of $H*$ is determined by the heat flow pattern from the hot walls to the cold walls. The positive and negative signs associated with $H*$ values represent counterclockwise and clockwise heat flow, respectively.

The heatlines in Figs. 6(a, b) are parallel to the two vertical boundaries at $x = 0$ and $x = \frac{\pi}{a}$, but perpendicular to the horizontal boundaries because conduction dominates near the boundaries. Unlike the isotherms, which are nearly horizontal during the initial phase of convection as shown in Fig. 3(b), the heatlines structures provide well-defined regions from which energy transfer occurs, as illustrated in Fig. 6(a). Furthermore, the heatlines are not perfectly parallel to the isotherms, as is expected at the onset of convection. The above results show that isotherms are not the best tools for visualizing and analyzing heat transfer during convection.

In the absence of the magnetic field, the heatlines are plotted for liquid gallium with $Pr_1 = 0.025$, as shown in in Figs. 6(c, d) for increasing values of thermal buoyancy $R = 3R_0$ and $R = 5R_0$, respectively. As $R$ increases from the onset (Fig. 6(a)) to three times of $R_0$, the intensity of heatlines also increases and semi-vertical lines deformed to many circular vortices near upper, lower as well as in central region with counterclockwise circulations. The transportation path of heatlines consists of a total of six vortices namely I-VI. The vortices I and II which lie near the lower boundary have circulations in opposite directions with extremum values of heat function as 71.23 and 65.71 respectively. The two small vortices, V and VI, that exist in the middle of the region near vertical walls have opposite circulation with the same intensity of 5.00. There also exist three more vertices III, VI and VII near the upper boundary with low heat function value. Heatlines are clustered near the hot lower boundary when compared to the upper cold boundary. It shows that most of the heat flux circulates near the bottom plate only and the transfer of heat to the top cold boundary is low. It is evident that the heatlines pattern is similar in both figures 6(c, d), i.e. as Rayleigh number increases from $R = 3R_0$ to $R = 5R_0$, the heatlines structure is almost same, but the absolute maximum and minimum values of heat flux increases from 71.23 and 65.71 to 360 and 340 respectively in the range of $0 < X < 1.4$.

For increasing values of $R$, heatlines are plotted in Fig. 7 in the presence of a vertically applied magnetic field. The magnetic field acts as a powerful resistance for fluid convection, so the trajectory taken by the heat flow to reach the cold wall is longer in the layer (($H^* = 0.33$)) for $Q = 0$ (Fig.6(a)) than for $Q = 670$. Such a heat flow analysis cannot be performed by using isotherms alone, as a result, isotherms are ineffective for visualizing and analyzing heat transfer. Figures 7(b,c) demonstrate the influence of increasing $R$ on heatlines in the presence of a vertically applied magnetic field. The heatlines in these figures appear more deformed than those in Fig. 7(a), indicating the start of convection. Figures 7(b, c) demonstrate that the heatlines are packed close to the lower boundary ($z = 0$), with higher values indicating large Nusselt numbers. The heatlines show an increase in heat transfer rate as $R$ increases due to the amplification of convective cells.

Figure 8 depicts the effect of increasing the value of $Q$ on the contours of heatlines. The heat transfer path to the cold wall is longer in the layer (($H^* = 0.33$)) for $Q = 670$ (refer fig. 7(a)) than for $Q = 1210$ (refer fig. 8(a)). The vertical heatlines in Figs. 8(b, c) are quite closer in the central region and the circulation diameters are small. It is evident that as the value of $Q$ increases, the flow circulation becomes less active, resulting in reduced convective heat transfer.

## 6. Conclusions

In this study, an analytical evaluation was performed to examine the fundamental physical process as well as interactions involved at the onset of convection in liquid gallium under the influence of an imposed vertical magnetic field. Further, the heat transport mechanism was also investigated under these conditions. Kuo [9] proposed an efficient perturbation method for studying nonlinear magnetoconvection. The effect of the thermal Prandtl number ($Pr_1$), magnetic Prandtl number ($Pr_2$), and the Chandrasekhar number ($Q$) were all considered to act simultaneously. Kuo [9] proposed the perturbation method and Rayleigh number ($R$ expansion) to obtain a set of non-homogeneous linear equations for temperature, velocity, and magnetic field. A general first-order solution of the equations of motion, temperature, and magnetic field was obtained for stress-free boundary conditions. The iterative method was used to derive the amplitudes up to the sixth order. The Nusselt number was evaluated and analysed up to the sixth order by using these solutions. It was observed that increasing $Q$ and $Pr_2$ has a dampening effect on the overall energy of the system. The convective heat transport and associated flow field have been explained for different values of $Q$ near the onset by utilizing the isotherms and streamlines, respectively. The results for a specific combination of the governing parameters, particularly for a related value of $Pr_1$ about liquid gallium a specific $Q$ value, revealed that as the magnetic field intensity increases, natural convection decreases. Convective motions in Rayleigh Benard convection are well known to be inhibited by an imposed magnetic field. These predictions were confirmed by the obtained results. It was also observed that the heat transfer decreased with increasing $Q$ in a uniform magnetic field. The results were visualised using heatlines and streamlines to demonstrate the convective heat transport and the nature of the fluid flow. In general, the results of convective heat transfer in liquid gallium have been reliably and conveniently discussed. The heat function results were found to be closely related to the average Nusselt number, which describes the heat transfer process. The patterns of heat lines obtained in this way described clearly defined corridors where energy transfer took place at the beginning of convection.

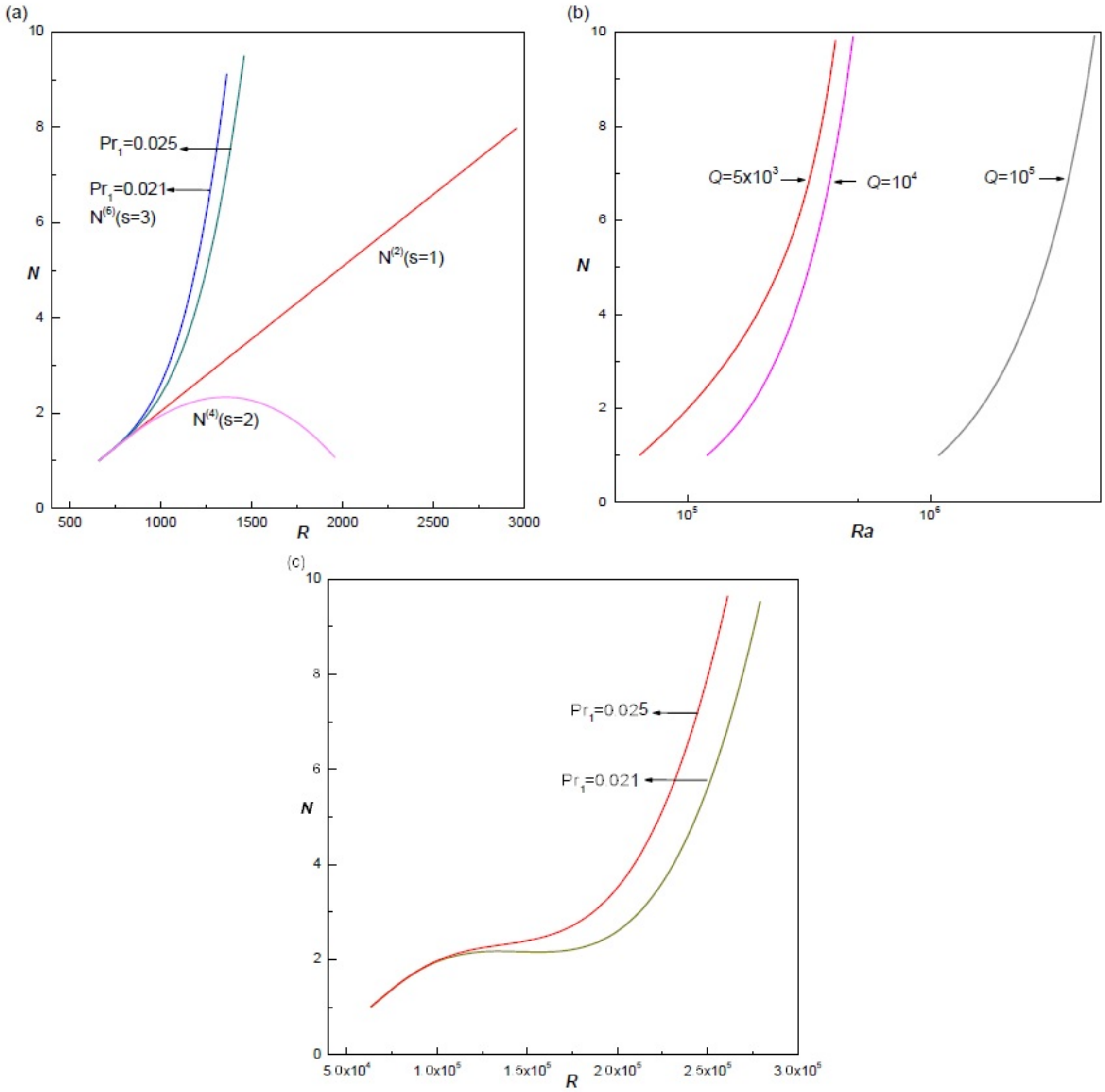


Figure 2: (a) This graph is plotted for $N$ versus $R$ for different $Pr_1$ and $Q = 0$. $N^{(2)}$, $N^{(4)}$, and $N^{(6)}$ are approximations of Nusselt number to the second (s=1), fourth (s=2), and sixth (s=3) orders, respectively. $N^{(2)}$ and $N^{(4)}$ are not dependent on $\boldsymbol{Pr_1}$ and $\boldsymbol{Pr_2}$. (b) Plotted for $N$ at sixth order ($N^{(6)}$) versus $R$ for various $Q$ with $Pr_1 = 0.025$ and $Pr_2 = 0.015 \times .10^{-6}$. (c) Plotted for $N$ versus $R$ for $Q = 5000$, with different $Pr_1$ and fixed $Pr_2 = 0.015 \times 10^{-6}$.

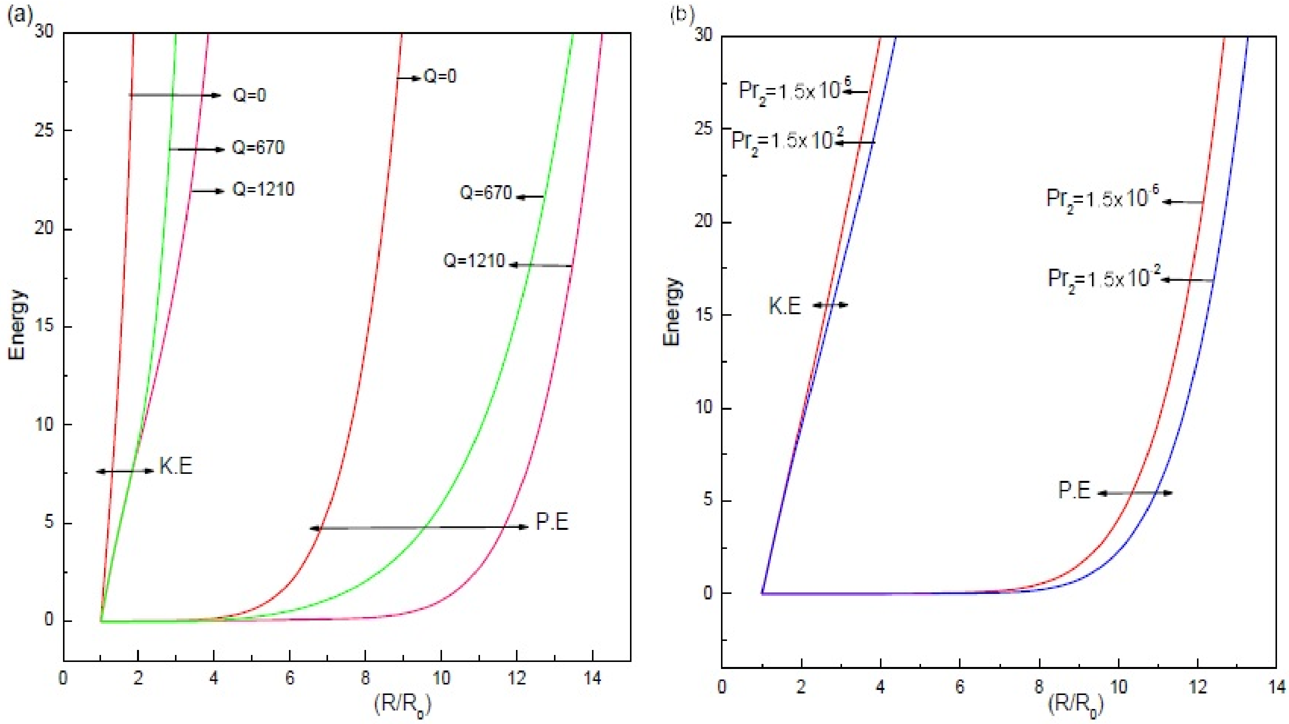


Figure 3: (a) Variation of kinetic and potential energy with respect to $R/R_0$ for different values of $Q$ for $Pr_1 = 0.025$ and $Pr_2 = 0.15 \times 10^{-6}$ (b) Variation of kinetic and potential energy with respect to $R/R_0$ for $Pr_1 = 0.025$, $Q = 5000$ with different values of $Pr_2$ .

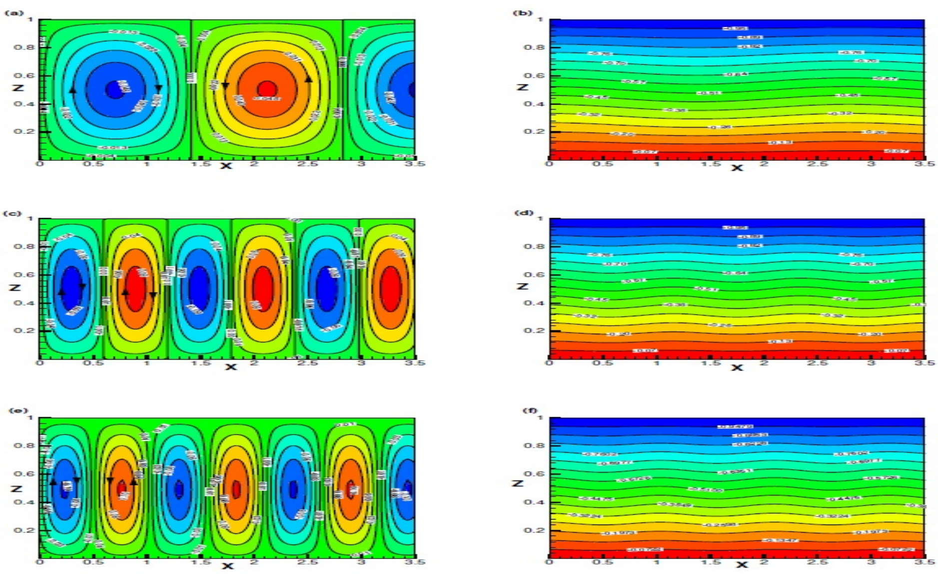

Figure 4: Effect of $Q$ for $Pr_1 = 0.025$ and $Pr_2 = 0.15 \times 10^{-6}$ at $R \simeq R_0$. Streamlines (a, c, and e). Isotherms (b, d, and f). Plots (a, b) for $Q = 0$, (c, d) for $Q = 670$, and (e, f) for $Q = 1210$.

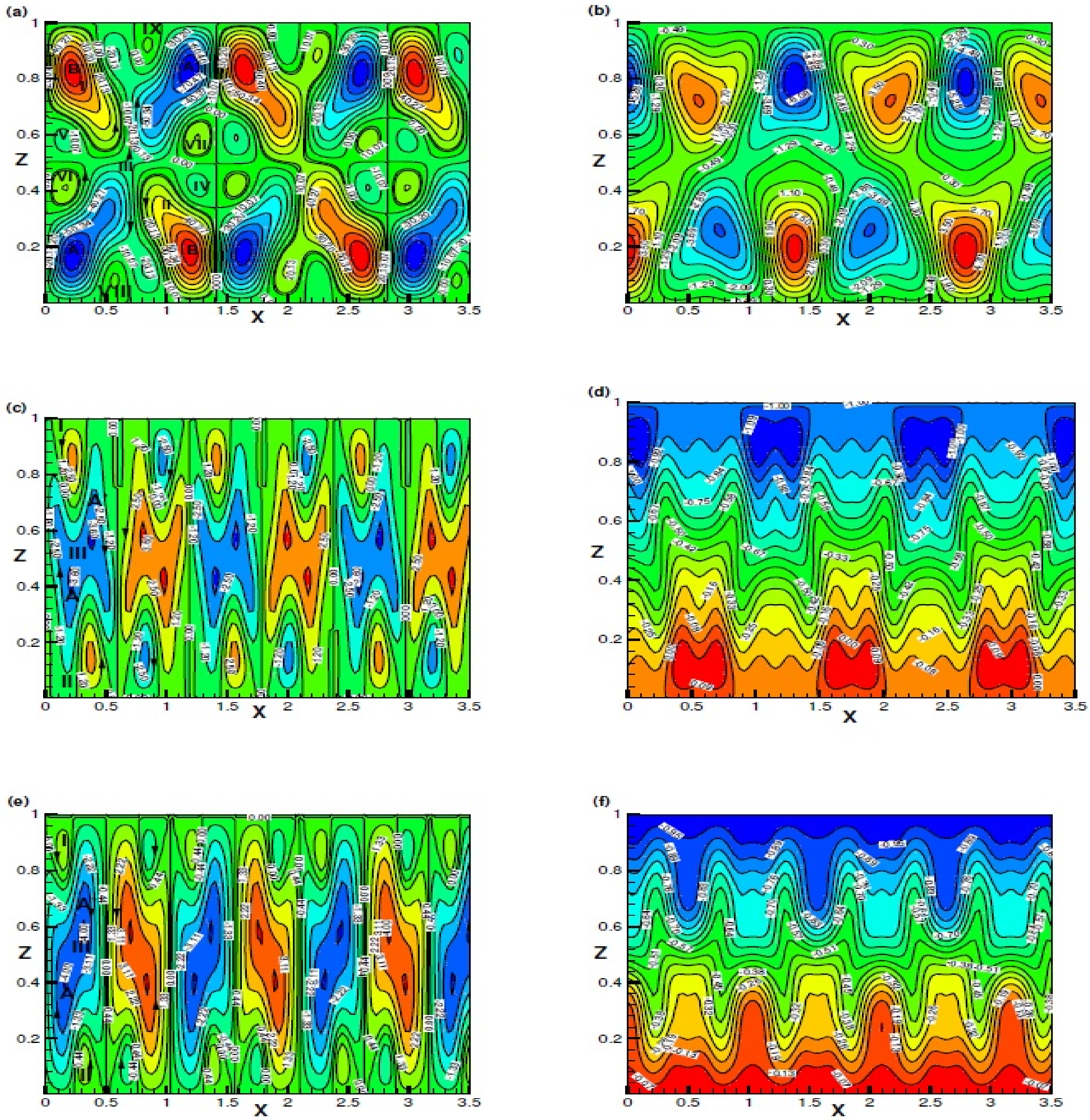

Figure 5: Effect of $Q$ for $Pr_1 = 0.025$ and $Pr_2 = 0.15 \times 10^{-6}$ at $R \simeq 3R_0$. Streamlines (a, c, and e). Isotherms (b, d, and f). Plots (a, b) for $Q = 0$, (c, d) for $Q = 670$, and (e, f) for $Q = 1210$.

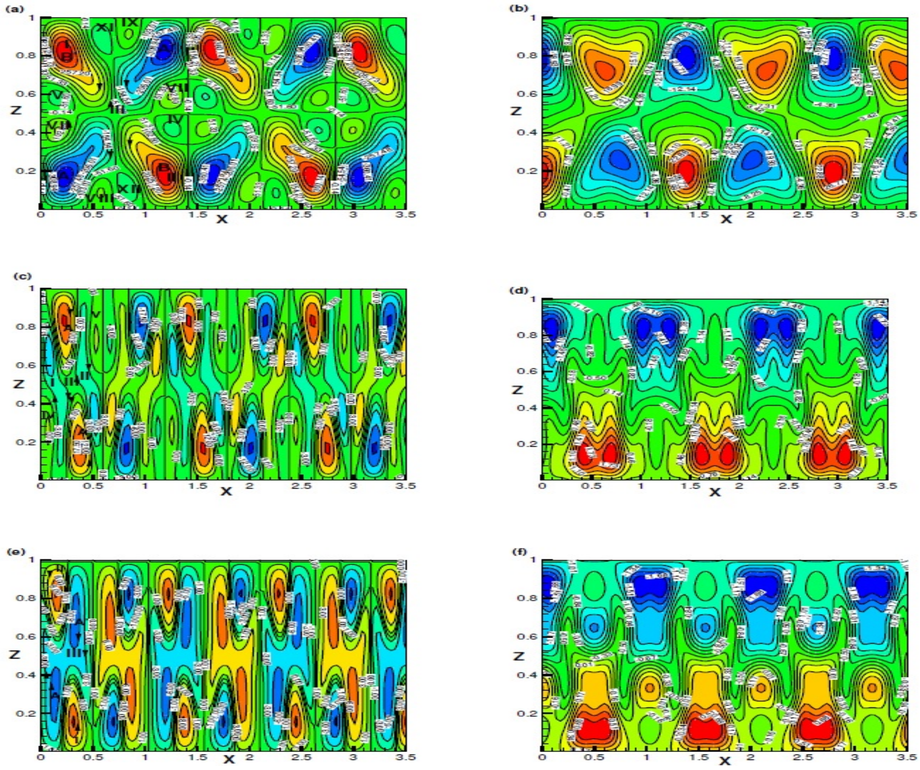


Figure 6: Effect of $Q$ for $Pr_1 = 0.025$ and $Pr_2 = 0.15 \times 10^{-6}$ at $R \simeq 5R_0$. Streamlines (a, c, and e). Isotherms (b, d, and f). Plots (a, b) for $Q = 0$, (c, d) for $Q = 670$, and (e, f) for $Q = 1210$.

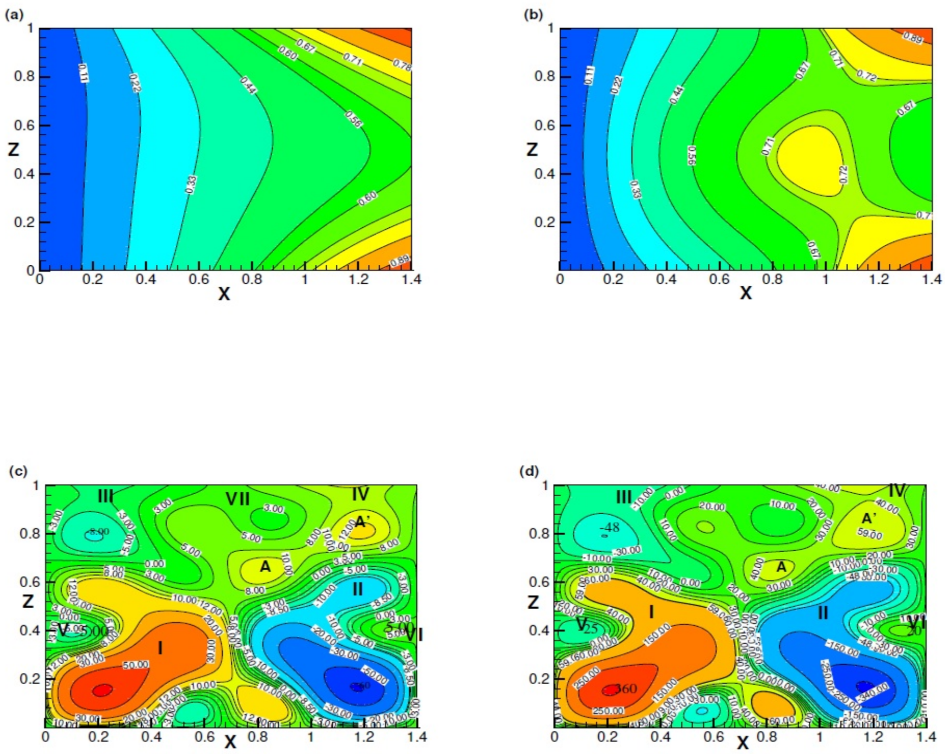


Figure 7: Heatlines for $Pr_1 = 0.025$; and $Q = 0$. (a) $T_o = 1$ and $R = R_0$, (b) $T_o = 3$ and $R = R_0$, (c) $R = 3R_0$ and $T_o = 1$ and (d) $R = 5R_0$ and $T_o = 1$.

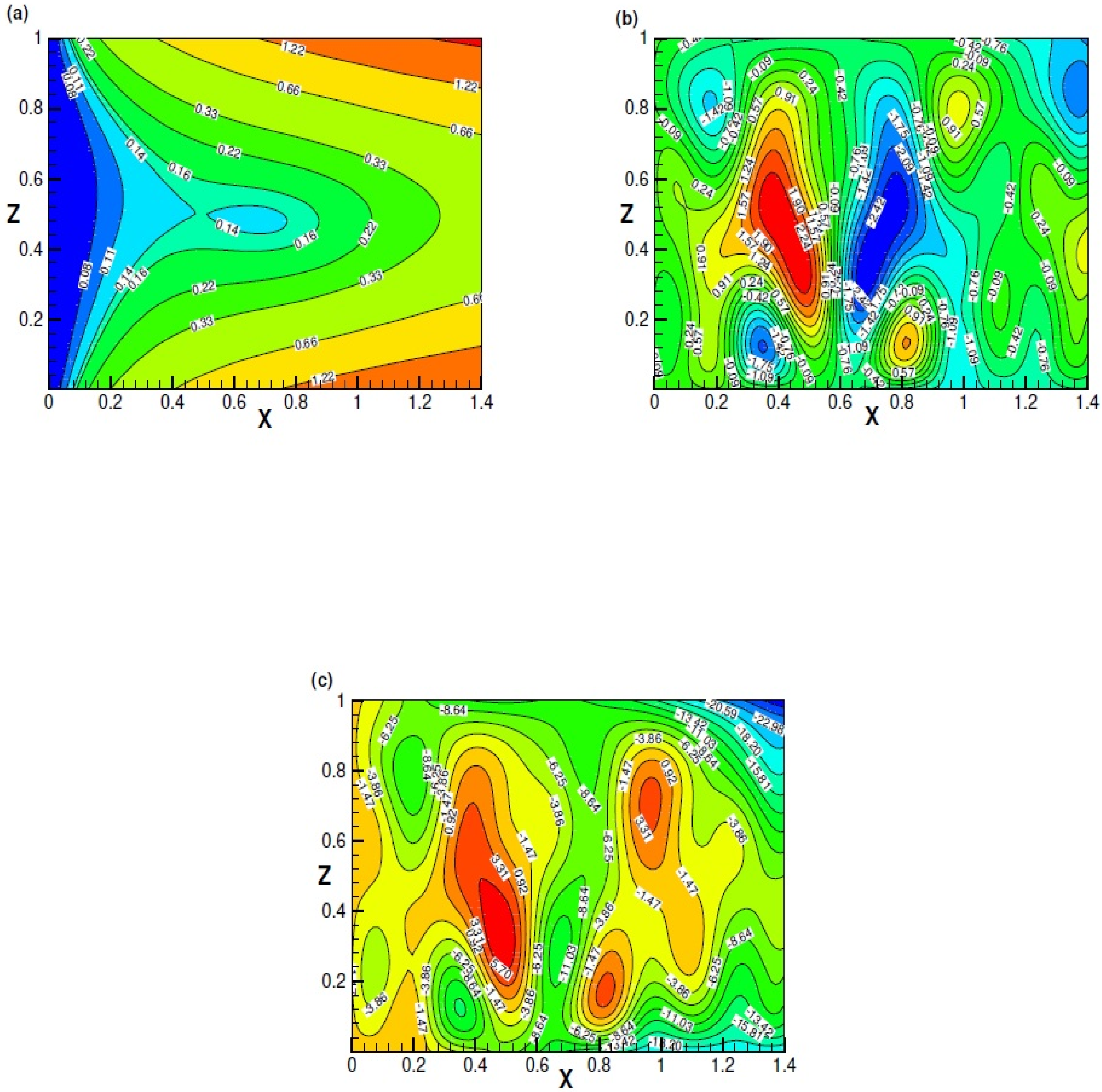

Figure 8: Heatlines for $T_o = 1$, $Pr_1 = 0.025$, $Pr_2 = 0.15 \times 10^{-6}$ and $Q = 670$. (a) $R = R_0$, (b) $R = 3R_0$, (c) $R = 5R_0$.

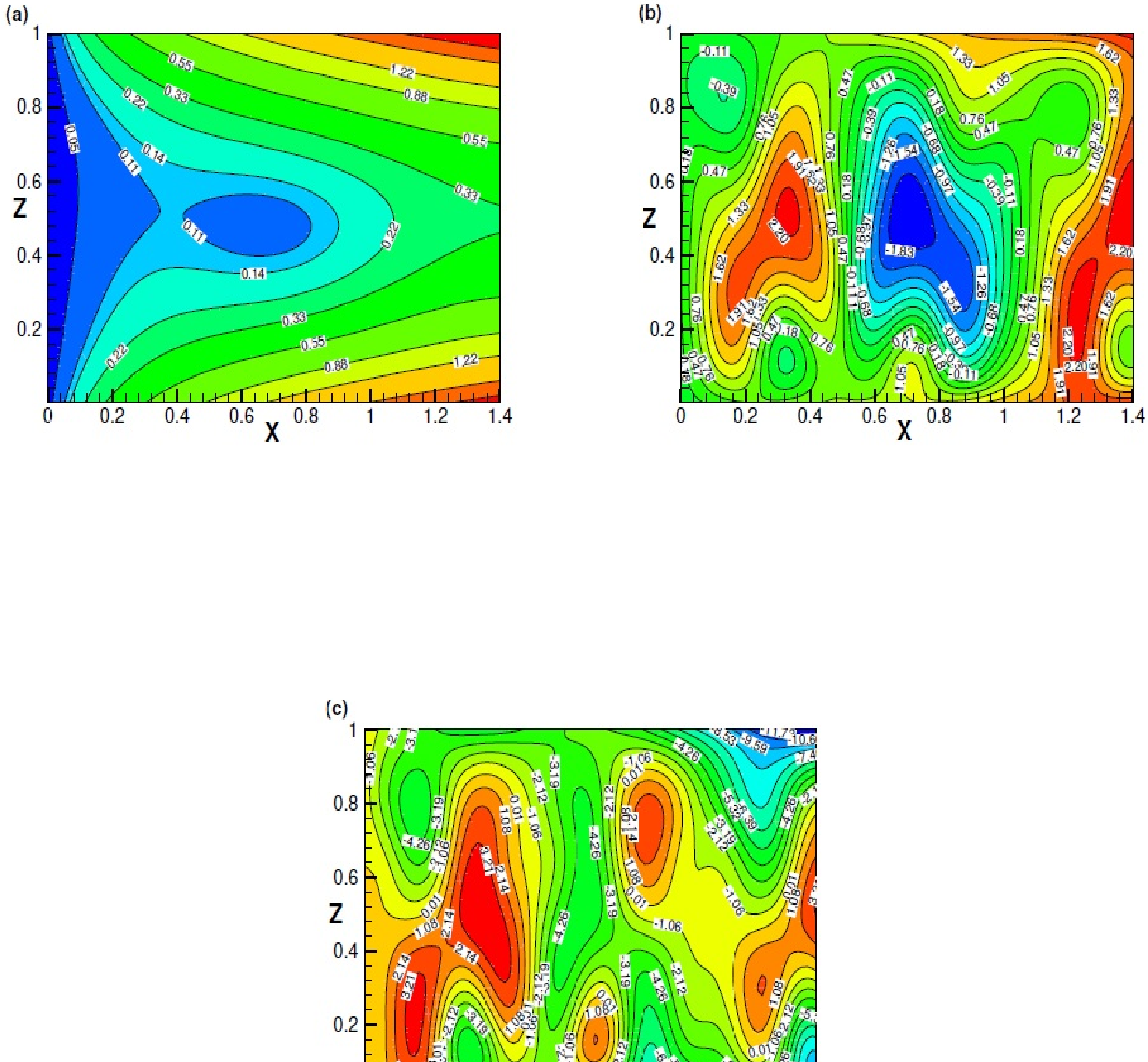


Figure 9: Heatlines for $T_o = 1$, $Pr_1 = 0.025$, $Pr_2 = 0.15 \times 10^{-6}$ and $Q = 1210$. (a) $R = R_0$, (b) $R = 3R_0$, (c) $R = 5R_0$.

## References

[1] Aurnou J. M., Olson P. L. Experiments on Rayleigh-Benard convection, magnetoconvection and rotating magnetoconvection in liquid gallium, J. Fluid Mech 430 (2001), 283–307.

[2] Chandrasekhar S. Hydrodynamic and Hydromagnetic Stability. Oxford University Press, 1961.

[3] Guray E., Tarman H. I. Thermal convection in the presence of a vertical magnetic field. Acta Mech. 194 (2007), 33–46.

[4] Jalil J. M., Murtadha T. K., AL-Tae'y K. A. Three dimensional computation of turbulent natural convection in the presence of magnetic field. J. Indian Inst. Sci. 86 (2006), 705–721

[5] Juel A., Mullin T., Ben Hadid H., Henry D. Magnetohydrodynamic convection in molten gallium. J. Fluid Mech 378 (1999), 97–118.

[6] Kenjeres S., Hanjalic K. Numerical simulation of magnetic control of heat transfer in thermal convection. Int. J. Heat Fluid Flow 25 (2004), 559–568.

[7] Kimura S., Bejan A. The heatline visualization of convective heat transfer. J. Heat Transfer 105 (1983), 916–919.

[8] Kloosterziel R. C., Carnevale G. F. Closed-form linear stability conditions for magneto-convection. J. Fluid Mech 490 (2003), 333–344.

[9] Kuo H. L. Solution of the non-linear equations of the cellular convection and heat transport. J. Fluid Mech. 10 (1961), 611–630.

[10] Kuo H. L. Power laws of high Rayleigh number convection. Boundary Layer Metero. 17 (1979), 29–39

[11] Nield D.A., Bejan A. Convection in Porous Media. Second ed., Springer, New York, 1999.

[12] Oreper G. M., Szekely J. The effect of an externally imposed magnetic field on buoyancy driven flow in a rectangular cavity. J. Crystal Growth 64 (1983), 505–515.

[13] Rameshwar Y., Rawoof Sayeed M.A., Rani H.P., Laroze D. Finite amplitude cellular convection under the influence of a vertical magnetic field. Int. J. Heat Mass Transfer 114 (2017), 559–577.

[14] Yanagisawa T., Yamagishi Y., Hamano Y. Structure of large-scale flows and their oscillation in the thermal convection of liquid gallium. Phys. Rev. E 82 (2010), 016321–016328.